Physical and mechanical properties of heat-damaged structural concrete containing expanded polystyrene syntherized particles

Francesco Lo Monte, Patrick Bamonte and Pietro G. Gambarova*,†

Department of Civil and Environmental Engineering, Politecnico di Milano, Milan 20133, Italy

Received 27 February 2013; Revised 31 October 2013; Accepted 21 December 2013

1. INTRODUCTION AND NATURE OF PROBLEM

Several papers have been published in the last decade on reduced-mass structural concrete containing synthetic particles and specifically expanded polystyrene syntherized (EPS) particles. The ensuing concrete is rather different from light-weight aggregate (LWA) concrete, as in EPS concrete the small EPS particles (that partially replace the medium and fine aggregates, with d_a below 8 mm) do not contribute to the mechanical properties of the material and—even worse—behave like small notches, while in LWA concrete, the fine and coarse light-aggregate particles give a non-negligible contribution to the mechanical performance (ACI 213R-87, [1]).

Expanded polystyrene syntherized concrete has been investigated for very different EPS contents, ranging from rather low fractions of the total volume (10%, [2]) to more than 50% [2–5] and up to 65% [6, 7]. However, only by limiting the EPS content by volume to less than 20%, it is possible to guarantee a suitable mechanical performance that according to [1] should not be below 17.2 MPa in terms of compressive strength on cylinders. As a matter of fact, the values comprised between 18 MPa [6, 7] and 40 MPa [8] are the most typical for EPS volume fractions from 15% to 20% of the total volume, with spikes in excess of 100 MPa [2] for very low values of the EPS fraction, which hardly justify the use of such light aggregates.

*Correspondence to: Pietro G. Gambarova, Department of Civil and Environmental Engineering, Politecnico di Milano, Milan 20133, Italy.

†E-mail: pietro.gambarova@polimi.it

The aforementioned relatively high values of the compressive strength come at the cost of huge cement contents, which span from 350 kg/m^3 [3] to 500 kg/m^3 [2], with spikes up to more than 800 kg/m^3 [2], not including silica fume and fly ash, which are often used to increase the strength and the workability of the mix (silica fume/cement ratio close to 10% by mass and fly ash/cement ratio from 0.30 to 1.00, see for instance [8, 9]). The water/cement ratio (or the water/binder ratio) is generally comprised between 0.35 and 0.60, with lows down to 0.2 [2]. Metallic fibers are used to increase concrete toughness (see for instance [4]), with fiber contents up to 70 kg/m^3 by mass (v_f close to 1% by volume).

Depending on EPS content (from 2.1 kg/m^3, [4], to 12.0 kg/m^3, [3]) and density (improved by syntherization, typically from 20 to more than 40 kg/m^3, see [4,8,10]), concrete density ranges from 550 kg/m^3 [6, 7] to 2000 kg/m^3 [2], but only in the range 1440–1850 kg/m^3 can EPS concrete be considered as a *light* and *structural* material, according to [1].

Expanded polystyrene syntherized generally is in the form of small spheres (called also *beads*, whose diameter is comprised between 3 and 8 mm, with a limited dispersion of the values with respect to the nominal value) or particles coming from reground EPS waste. (Other hollow particles suitable as a partial replacement of ordinary aggregates should be mentioned, like the *cenospheres* produced by the coal-burning plants and proposed by Blanco *et al.* [11]; diameter = 1.5–2 mm; density = 1100–1500 kg/m^3; f_c up to 30 MPa).

In terms of mechanical performance, the compressive strength and the elastic secant modulus are linearly decreasing functions of both the EPS content by volume [3] and of concrete density, while the tensile strength by splitting decreases less than linearly [4]. Silica fume increases the adhesion between EPS particles and concrete [4], while fly ash decreases water absorption and moisture migration [5].

Numerically modeling the microstructure of EPS concrete allows to enhance its mechanical performance, by optimizing the packing of the particles and the strength of the matrix [12, 13]. The particle-related size effect has been investigated by Miled *et al.* [2,14], who explained the lack of size effect at very high porosity levels (i.e., when the concrete contains many small EPS particles).

Today, the driving force behind the renewed interest for cementitious composites containing EPS particles is *materials recycling for sustainable constructions* [10], because EPS particles come generally from ground polystyrene waste. By partially replacing medium and fine aggregates with EPS particles, a second objective is achieved, as concrete mass per unit volume can be reduced by 10–20%.

Unfortunately, for the same cement content, EPS-based concretes exhibit lower mechanical properties than ordinary and LWA concretes (the latter containing expanded clay, shale, or slate). Whenever other light aggregates are not available, however, granulated EPS becomes a viable alternative for the construction of floors, curtain walls, shell roofs, folded plates, fire walls, load-bearing and not load-bearing partitions, and in the prefabrication industry [8].

With specific reference to the behavior of reinforcement-concrete bond in R/C members made of EPS concrete, some tests have been recently performed at the University of Sannio (Benevento, Italy) on three mixes, a reference mix and two mixes containing EPS particles, with a compressive strength on cylinders comprised between 17 and 25 MPa [15]. A research project on similar but higher grade mixes has been lately completed in Milan (f_c = 25–30 MPa, [16]), with reference to high temperature (T = 20°C, 150°C, 300°C, 500°C, and 700°C), in order to investigate the mechanical properties of EPS concrete *after cooling* (*residual* strength in compression and in indirect tension by splitting, and *residual* elastic modulus), as well as the mass per unit volume and the thermal diffusivity as a function of the temperature. As no results are available in the literature on EPS concrete exposed to high temperature, the tests carried out in Milan are meant to shed some light on the high-temperature behavior of this material, which may be affected both favorably and unfavorably by EPS melting (at 100°C), decomposition (at 230–270°C), and ignition (at 450–500°C). In fact, these phenomena lead to the formation of further porosity (which favors the release of water and vapor pressure in the capillary pores, to the advantage of concrete mechanical properties), but at the same time, the burning of polystyrene particles (whose volume is occupied for more than 95% by air) may create dangerous pressure peaks.

2. MIX DESIGN AND COMPRESSIVE STRENGTH OF THE VIRGIN MATERIALS

The constituents and the main physical and mechanical properties of the three concretes investigated in this project are summarized in Table I. Note that Mix M1 is rather typical, being close—for instance—to Mix 1 of [8], while Mix M2 is rather untypical for its very high cement content, but it is close to the Mix M_1–10 tested in [2].

The choice of the mixes was dictated by the requirement that the compressive strengths of the reference mix (Mix M0) and of the first EPS mix (Mix M1) were the same, while the third mix (Mix M2) was intended to explore to what extent adding cement would increase the strength. (The cement content in Mix M2 is roughly 25% larger than in Mix M1).

The specimens were cured for 28 days in controlled conditions ($T = 22°C$ and R.H. $\geq 95\%$) and then were kept for 2 months in normal conditions ($T = 20$–$25°C$, R.H. = 70–80%). The compressive strength on cylinders was measured both at 28 and at 90 days (Table I). Heating, cooling, and testing started 3 months after casting and were completed in the subsequent 2 months.

3. SPECIMENS, THERMAL CYCLES, AND INSTRUMENTATION

For each mix, 11 cylinders were cast, that is, 10 for the tests in compression and 1 for the tests in indirect tension by splitting (Figure 1). In this way, two cylinders were available for each of the five reference temperatures ($T = 20°C$, 150°C, 300°C, 500°C, and 700°C, Figure 2(a)). Among the 11 cylinders, two were *large* ($\varnothing = 150$ mm, $h = 300$ mm; tests at 20°C), while nine were *small* ($\varnothing = 100$ mm, $h = 200$ mm; tests at high temperature in compression and tests in indirect tension, Figure 1(a) and (b)). One of the small cylinders was instrumented with two thermocouples to evaluate the thermal diffusivity up to 700°C. After cooling down to room temperature, this cylinder was tested as well, because it had reached the reference temperature of 700°C. For each mix, six thick disks ($\varnothing = 100$ mm; $t = 40$ mm) were cut from the 11th small cylinder, for the splitting tests at $T = 20°C$, 300°C, and 600°C.

All the tests in compression were displacement controlled. The shortening of the specimens was measured via three resistive gauges placed at 120° astride the mid-height section (base length 100 mm, see DD1 in Figure 1(a)); moreover, three linear variable differential transformers measured the plate-to-plate distance of the press to monitor the post-peak behavior of the specimens. In all the tests in compression, stearic acid was smeared on the end sections of the specimens to reduce plate-to-concrete friction.

The tests by splitting were force controlled, and an electromechanical press INSTRON was used (capacity 100 kN).

Table I. Mix design, mass per unit volume, and compressive strength of the three concretes.

Concrete Mix	M0 (reference)	M1	M2
Cement CEM II A-LL R 42.5 (c) (kg/m^3)	286	643	815
Mixed aggregates = Sand + gravel (kg/m^3)*	809 + 1006	475 + 591	620 + 310
Water (kg/m^3) [w/c]	200 [0.70]	220 [0.34]	220 [0.27]
Expanded polystyrene syn. beads (EPS) (kg/m^3)**	—	5.09	5.32
Super plasticizer (sp) (kg/m^3) [sp/c]	3.90 [1.4%]	7.05 [1.1%]	9.11 [1.1%]
Air-entraining agent (ae) (kg/m^3) [ae/c]	—	2.12 [0.33%]	2.73 [0.33%]
Viscosity modifier (vm) (kg/m^3) [vm/c]	3.90 [1.4%]	7.05 [1.1%]	9.11 [1.1%]
Nominal mass/actual mass (kg/m^3)	2309/2239	1951/1899	1991/1951
Compressive strength at 28 days(MPa)	23.5	24.7	26.3
Compressive strength at the beginning of the tests (at 90 days, MPa)	25.8	26.9	28.4

*Max aggregate size $d_a = 12$ mm; the aggregates were in water-saturated surface-dry conditions.
**3 mm beads; mass per unit volume = 38 kg/m^3 after syntherization; EPS volume fraction = 13.5–14%.

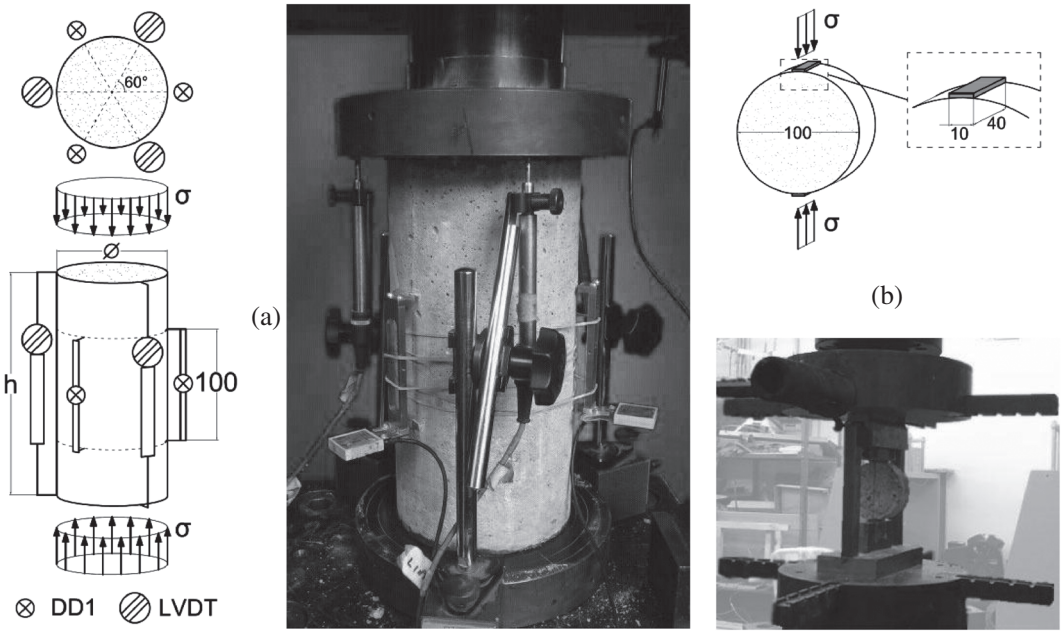

Figure 1. Typical specimen ready to be tested in compression (a) and in tension by splitting (b).

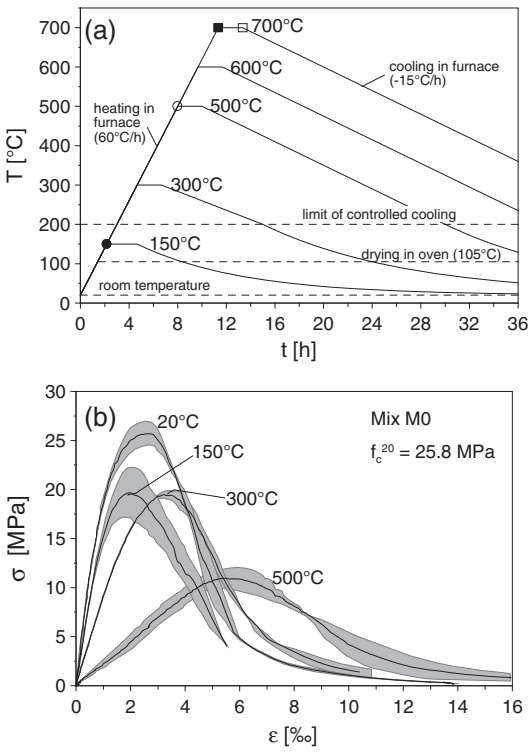

Figure 2. Thermal cycles at 150°C, 300°C, 500°C, and 700°C for the tests in compression, 300°C and 600°C for the tests in tension (a) and example of test repeatability in compression for Mix M0 (b).

The elastic modulus was evaluated from the stress–strain curves in compression, as *secant modulus* ($\sigma_c \leq 0.5 f_c$). Prior to being tested, all specimens were subjected to ultrasounds to measure the velocity of the longitudinal waves (v_{us}), which decreases with the temperature and is instrumental in formulating a *damage index*, as mentioned in the last chapter before the conclusions.

All the specimens were slowly heated to the reference temperature (heating rate = 1°C/min) and rested at that temperature for 2 h, to guarantee the uniformity of the thermal field (Figure 3(d)). Then, the specimens were slowly cooled down to 200°C at −0.25°C/min and to 20°C in natural conditions (inside the closed furnace). The symbols ● ○ ■ □ in Figure 3(a)–(d) refer to the instants when the temperatures were measured during the thermal cycles (Figure 2(a)).

Note that the limited number of the specimens (two per each reference temperature) does not diminish the reliability of the results, because in all cases, the repeatability of the tests was excellent, as it is shown in Figure 2(b) for Mix M0. (Note that in the case $T = 150$°C, the scattering is due to the complex phenomena accompanying water evaporation between 100°C and 200°C, with pressure peaks in the pores of the cementitious matrix; at higher temperatures, the hydration of the anhydrous cement—*cement rehydration*—and the improvement of the bonding properties of the newly formed hydration products reduce concrete heat sensitivity, [17]).

4. MOISTURE CONTENT AND MASS PER UNIT VOLUME

The largest pieces of the specimens tested in compression were placed for 2 weeks inside an oven at 105°C, in order to measure the stabilized mass after the loss of the free water (Figure 4(a)). In the case of Mix M0, mass stabilization was reached in 1 week, with a normalized moisture loss close to 3%, while EPS mixes required more time (twice as much), and their mass loss was definitely higher, between 5.3% (Mix M1) and 5.7% (Mix M2). These higher losses before mass stabilization are confirmed by those observed in a previous research project on two light-weight concretes and on a reference concrete kept at 105°C for 1–2 weeks (LWC/HPLWC/NSC: $\rho_c = 1809$, 1920, and 2300 kg/m^3, $f_c = 39/56/30$ MPa, mass loss = 8/10/4%, [18]). The reason

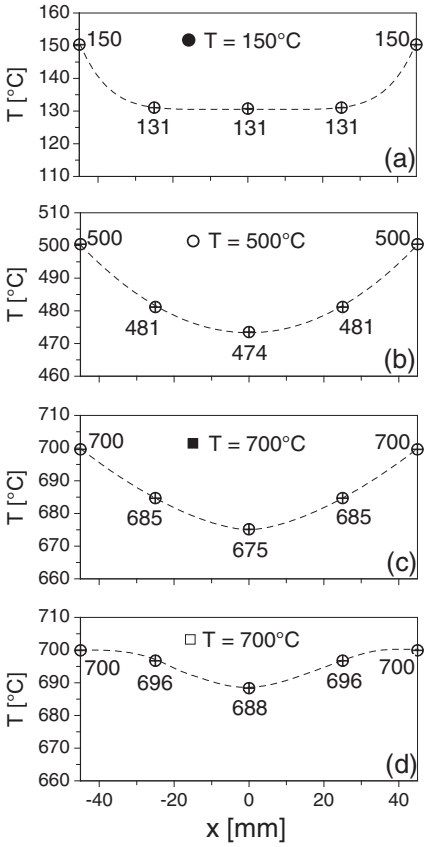

Figure 3. Typical temperature profiles in the mid-span section of a cylinder ($h = 2\varnothing = 200$ mm), Mix M0, $T = 150$°C (a); 500°C (b); and 700°C (c,d); $\Delta T/\Delta t = 1$°C/min. For ● ○ ■ □, see Figure 2a.

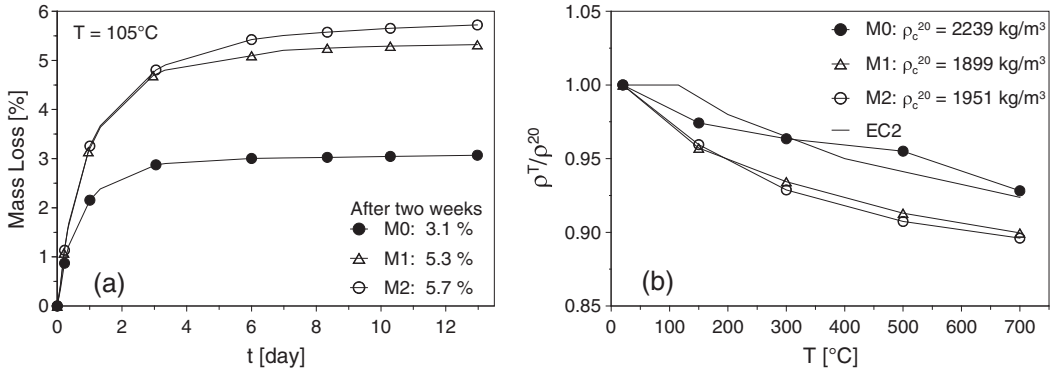

Figure 4. Mass decrease due to free-water expulsion at 105°C (a), as a function of time, and mass loss at high temperature (b), as a function of temperature.

why concrete containing expanded clay or EPS aggregates loses more than ordinary concrete is mostly because in the former case, the light aggregates are porous and retain water so that their saturation water is more than in ordinary concrete, while in the latter case (EPS-based concrete), some water remain entrapped at the interface between the EPS particles and the concrete, and it is expelled during the heating process.

As for the mass evolution at high temperature, all specimens to be tested in compression were weighed before and after the thermal cycle, and the plots of the average mass loss (measured on two specimens for each reference temperature and mix) are plotted in Figure 4(b) for the three mixes. Mix M0 loses 4.5% at 500°C and 7.2% at 700°C, while Mixes M1 and M2 lose roughly 9.0% and 10.2% at the same temperatures. On the whole, however, the mass loss induced by the temperature is similar to that predicted by EC2—Fire Design [19] for ordinary concrete (see the continuous curve in Figure 4(b)).

5. POROSITY

5.1. Total porosity

The porosity was investigated by means of two well-known techniques based on mercury intrusion (mercury intrusion porosimetry, MIP) and water absorption (water absorption porosimetry, WAP, according to ISO 5017 [20]), at room temperature and after heating to 300°C and 600°C. Both techniques allow to evaluate the total porosity, but the former gives also information about pore-size distribution. Preliminarily, the specimens were dessiccated in an oven at 80°C. (The usual temperature of 105°C would have caused the partial melting of the polystyrene particles).

Before looking at the evolution with the temperature, one should remember that WAP generally yields higher values than MIP in terms of total porosity because of the small size of the water molecules, which penetrate more easily into the pores and specifically into the nanopores [21].

For the three mixes, the total porosity evaluated by means of MIP (Figure 5(a)) increases regularly with the temperature and—as expected—is lower than the porosity measured by means of WAP (Figure 5(b)), at any temperature for Mix M0, and above 300°C for Mixes M1 and M2. On the contrary, the total porosity evaluated by means of WAP exhibits a sharp increase between 20°C and 300°C for Mixes M1 and M2. Both the regularity of the porosity yielded by MIP and the rather odd behavior of the porosity yielded by WAP (Mixes M1 and M2) can be explained in the following way:

- because of the high pressure used in MIP (up to 200 MPa), the mercury tends to fill not only the volume of the micropores but also that of the EPS particles, be they undamaged but very soft ($T = 20$°C), melted, or gassified ($T = 300$°C and 600°C); hence, the initial porosity is rather high and tends to remain almost constant (Mix M1 and—to a lesser extent—Mix M2), while the much lower values of Mix M0 indicate a sort of linearity with the temperature, see Figure 5(a);

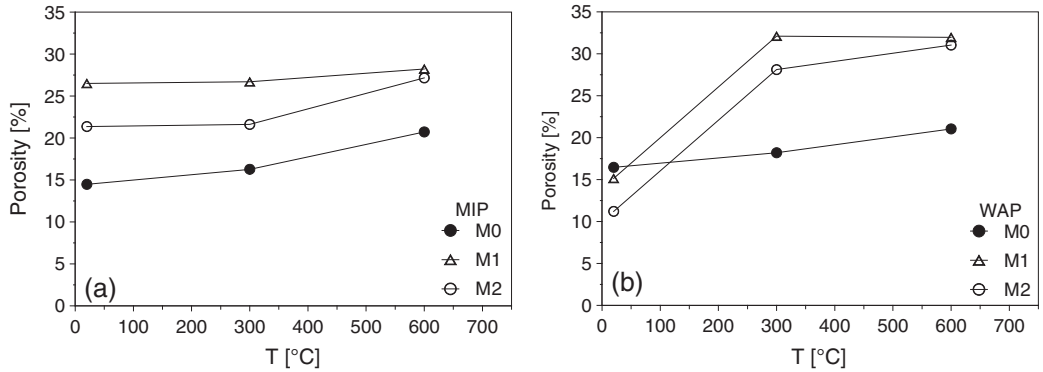

Figure 5. Plots of the porosity according to mercury intrusion porosimetry (MIP) (a) and to water absorption porosimetry (WAP) (b).

- the initial values of the porosity measured by means of MIP result from the sum of the porosity of the cementitious matrix (10–15%) and of the volume of the EPS particles (13–14%), see Figure 5(a);
- because EPS is hydrophobic, the water used in WAP does not fill the volume of the EPS particles at 20°C in Mixes M1 and M2; hence, the porosity tends to be similar to that of Mix M0 at 20°C, and only after the disappearance of the EPS particles (at and above 300°C, see the black spots representing the voids, Figure 6) can the water fill the voids left by the EPS particles, with a sudden increase of the porosity between 20°C and 300°C, see Figure 5(b);
- the rather small increase of the porosity between 300°C and 600°C is mainly because of thermal microcracking and to the expulsion of the bound water; the closeness of the values of the porosity above 300°C confirms the reliability of the measures obtained in two different ways, MIP and WAP.

5.2. *Pore-size distribution*

As already mentioned, MIP allowed to investigate pore-size distributions, which clearly indicate a tendency for the pores to become larger and larger at increasing temperature, in all mixes (Figure 7).

In detail, Mix M0 exhibits a regular increase of the porosity (Figure 7(a)), whatever the pore size, with a marked increase of the largest pores (5 μm) after the exposure to 600°C. The same occurs in Mixes M1 and M2 (Figure 7(b) and (c)) with the peaks of the porosity moving from 30 nm to 30 μm after the exposure to 600°C. As previously indicated by the total porosity, at room temperature, both Mixes M1 and M2 exhibit a much larger porosity than Mix M0, in the range 20 nm–30 μm.

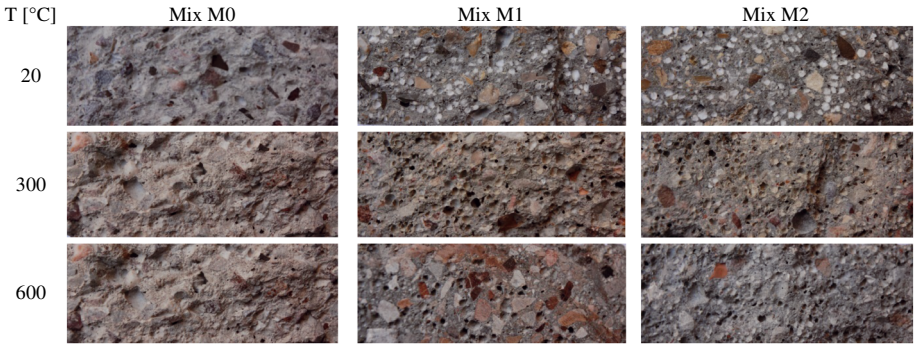

Figure 6. Pictures of the fractured sections of the specimens for $T = 20$°C (the white spots represent the EPS particles in Mixes M1 and M2) and after heating to 300°C and 600°C (the voids left by the melted and gassified EPS particles appear as black spots).

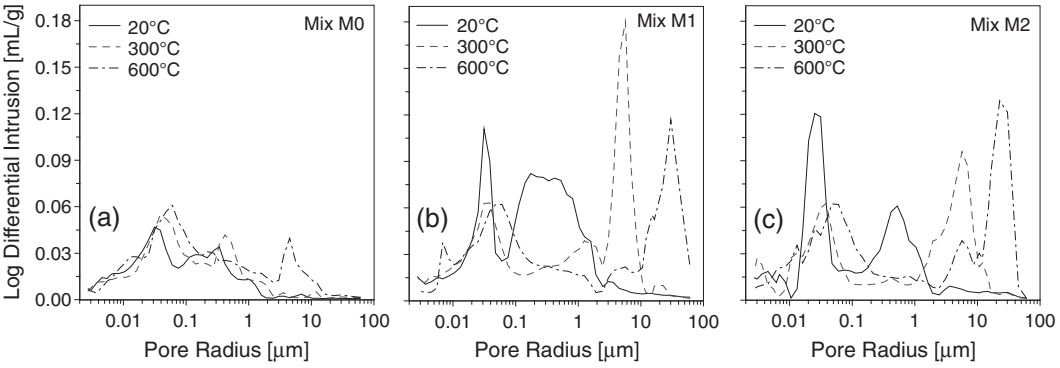

Figure 7. Plots of the differential intrusion (in log scale) as a function of pore radius. (a) Mix M0; (b) Mix M1; and Mix M2 (c).

6. THERMAL DIFFUSIVITY

The thermal parameter controlling heat transmission by conduction is the thermal diffusivity, which is the ratio between the heat transmitted and the heat stored by the unit mass of the material in question. (The smaller the thermal diffusivity, the higher the insulation ability). The thermal diffusivity is defined as $D = \lambda/(c\ \rho)$, where λ is the thermal conductivity, c is the specific heat, and ρ is the mass per unit volume. In a long cylinder ($h \geq 2\varnothing$) subjected to a constant heating rate (v_h = mean heating rate inside the specimen, [22]), the thermal diffusivity can be evaluated by means of the following equation:

$$D = v_h R^2/(4\ \Delta T) \tag{1}$$

where $\Delta T = T_2 - T_1$ is the difference between the temperatures measured in two points (at—or close to—the surface and along the axis in the mid-span section), while R is the distance between the two points.

Three cylinders—one for each mix—were instrumented with two thermocouples and slowly heated from 20°C to 700°C; T_1 and T_2 were measured at regular intervals. As shown in Figure 8(a), between 250°C and 500°C, the thermal diffusivity of the three concretes is roughly constant (=0.30–0.45 mm^2/s in Mix M0). At 250°C, adding EPS decreases the thermal diffusivity by -20% to −40% compared to ordinary concrete (full curve in Figure 8(a)), and at 500°C, the difference is still close to −15% to −20%. Furthermore, for Mixes M1 and M2, the thermal diffusivity is very close to that of two light-weight expanded clay concretes tested by the second and third authors in a previous project (Figure 8(b), LWC/HPLWC/NSC, [18]). Hence, EPS concrete has the same good insulation properties as expanded clay concrete.

The rather sharp downward spikes at 150–200°C and 550°C are due to two endothermic phenomena: (1) the change of state of the water from liquid to vapor in the micropores and (2) the change in the crystalline system (from α to β) of the quartz contained in the fine aggregates.

Last but not least, EPS melting at 100°C, decomposition at 230–270°C, and ignition at 450–500°C do not seem to affect the thermal behavior of EPS concrete; as already mentioned, however, above 300°C, the EPS beads are gone, and their empty volumes are clearly visible on any fractured or free surface (Figure 6).

The very good insulation properties of EPS concrete allows to reduce the net cover of the rebars in R/C structures or to increase the fire resistance for the same cover, as shown in the simple example of Figure 9(a), where a typical bar embedded in EPS concrete (M1) reaches the *critical temperature* of the steel (400°C) after 120 min, while the same bar embedded in ordinary concrete (M0) reaches the same temperature in 95 min (the fire resistance is reduced by 21%). Conversely, after a 95-min fire (Figure 9(b)), the temperature of the bar embedded in EPS concrete is 340°C, that is, 18% lower than the temperature in the bar embedded in ordinary concrete (400°C).

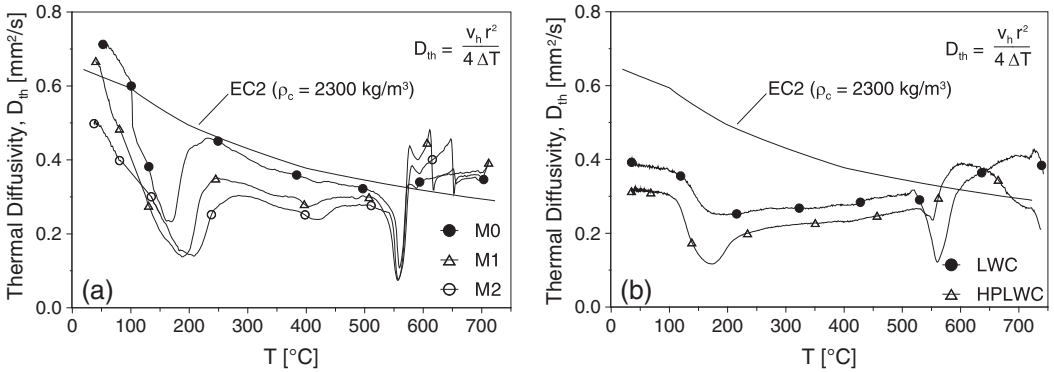

Figure 8. Thermal diffusivity: EPS concrete (a) and expanded clay concrete (b) [18]. The thick curve is based on the lower curve provided by EC2 [19] for the thermal conductivity.

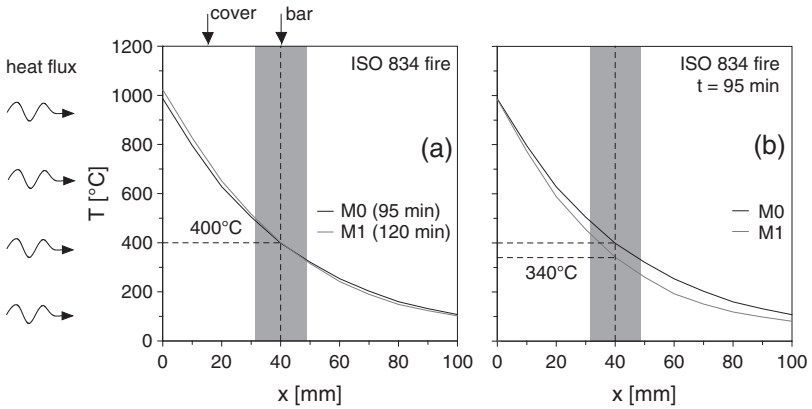

Figure 9. Temperature profiles in a R/C slab subjected to the standard fire (ISO 834 or ASTM E 119), made of either EPS concrete (M1) or ordinary concrete (M0): (a) same bar temperature (400°C), different fire duration; and (b) same fire duration (95 min), different bar temperature. Bar diameter $\varnothing$ = 16 mm; net cover = 2 $\varnothing$ = 32 mm.

7. RESIDUAL MECHANICAL PROPERTIES

The stress–strain curves in compression are plotted in Figure 10; all are characterized by well-defined linear loading branches, nonlinearities more or less pronounced close to the peak and descending branches, but Mix M0 is definitely tougher, with rather rounded peaks and a regular softening, at any temperature, while Mixes M1 and M2 are more brittle, with a rather steep softening up to 500°C. Mix M0 is the only one to exhibit a plateau between 150°C and 300°C, with no change in terms of peak stress, something often found in ordinary aggregate normal-strength and high-performance concretes.

The normalized plots of the strengths in compression and in indirect tension by splitting are reported in Figure 11(a) and (b), respectively. Mixes M0 and M2 closely adhere to ACI curves [23] for the residual compressive strength, as the measured values are generally comprised between the curves given for carbonate and siliceous aggregates, respectively (Figure 11(a)), while Mix M1 seems to be the most temperature sensitive at any temperature.

As expected, the tensile strength (Figure 11(b)) is slightly more temperature sensitive than the compressive strength, but there are no sizable differences among the three mixes.

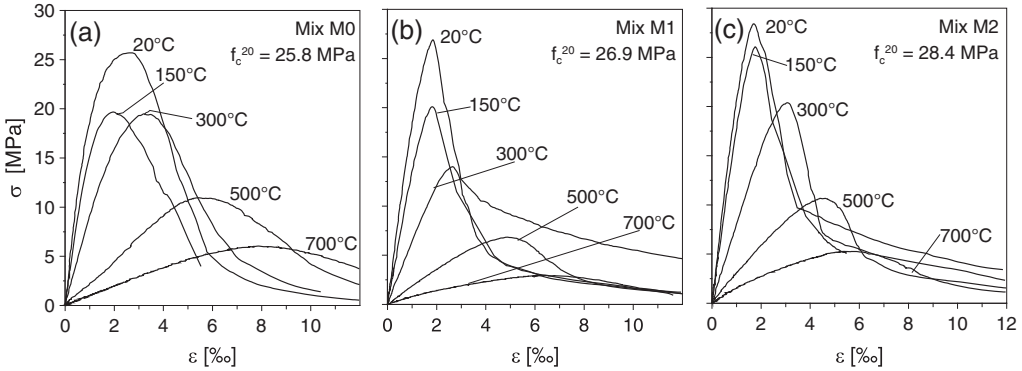

Figure 10. Stress–strain curves in uniaxial compression. (a) Mix M0; (b) Mix M1; and Mix M2 (c).

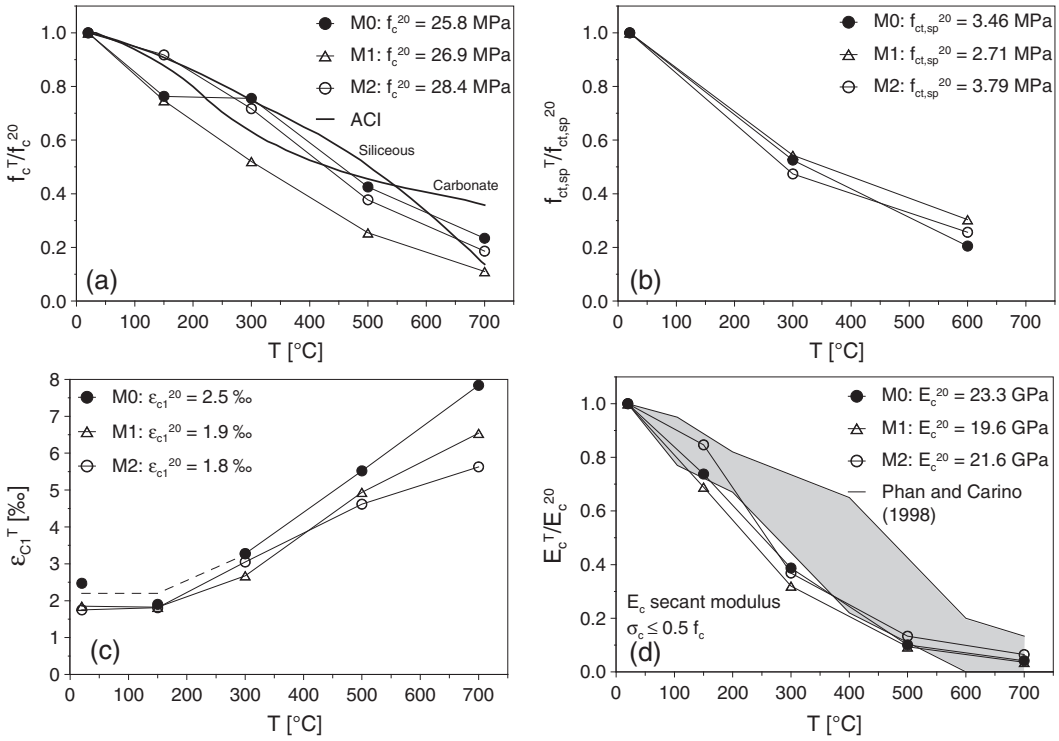

Figure 11. (a,b) Normalized plots of the compressive strength and of the indirect tensile strength by splitting; (c) plots of the strain at the peak stress; and (d) normalized plots of the secant elastic modulus.

As for the strain at the peak stress (Figure 11(c)), the values are comprised between 1.8‰ and 2.5‰ at 20°C (from Mix M2 to Mix M0) but jump to 5.5‰ and 8.0‰ at 700°C.

In terms of normalized elastic modulus, the heat sensitivity of EPS concrete is hardly different from that of ordinary concrete, as shown in Figure 11(d), where the cloud of the test results examined in [24] is reported. Mix M1, however, is again the most heat sensitive.

It should be observed that increasing the cement content beyond certain limits hardly improves the mechanical performance at any temperature (compare Mix M2 and Mix M1).

As already observed, not only EPS concrete has generally a lower mechanical strength than ordinary concrete in terms of compressive strength but also the elastic modulus is much lower (at 20°C, from −10% to −15% with respect to an ideal equally dense ordinary concrete). Although the data base is very limited, there are indications that EPS concrete is more temperature sensitive than ordinary concrete in terms of compressive strength, unless large cement contents are used.

8. DAMAGE INDEXES

Temperature-induced damage in quasibrittle materials—mainly in the form of microcracking and porosity—can be quantified by means of *damage indexes*, generally indicated with D ($D = 1 =$ fully damaged material or failure of the material; $D = 0 =$ no damage in the material). Damage indexes were first introduced in the 1970s of the past century, and among the parameters controlling the damage, the elastic modulus, the density, the ultrasonic velocity, the stress amplitude, the strain rate, and the hardness were introduced by various researchers (see for instance [25]), to quantify the effect of loading, with reference to material stiffness, ductility, creep behavior, and low-cycle/high-cycle fatigue resistance.

In the case of fire-damaged concrete, a possible use of damage indexes based on the elastic modulus was proposed in [26, 27], as a means to assess the fire-induced damage in different concretes.

Among the previously indicated damage indexes, those based on the elastic modulus E ($D_E{}^T$, Equation 2) and on the velocity of the ultrasonic waves v_{us} ($\tilde{D}_v{}^T$, Equation 3) are rather popular:

$$D_E{}^T = 1 - \left(E^T / E^{20}\right) \tag{2}$$

$$\tilde{D}_v{}^T = 1 - \left(v_{us}{}^T / v_{us}{}^{20}\right)^2 \tag{3}$$

It should be observed that both the elastic modulus and the velocity of the ultrasonic waves are decreasing functions of the temperature (Figures 11(d) and 12).

Because in an elastic continuum the elastic modulus is proportional to the square of the velocity of the ultrasonic waves times the mass per unit volume ρ, the damage index based on the ultrasonic velocity can be reformulated as follows:

$$D_v{}^T = 1 - \left(\rho^T / \rho^{20}\right) \bullet \left(v_{us}{}^T / v_{us}{}^{20}\right)^2 \tag{4}$$

Note that in a perfectly elastic continuum, (E^T/E^{20}) and $[(\rho^T/\rho^{20}) \bullet (v_{us}{}^T / v_{us}{}^{20})^2]$ coincide (if the dependence of the Poisson ratio on the temperature is neglected), while in an actual (inelastic) continuum, the results are more or less different, depending on the definition of E. (Slope E_0 of the stress–strain curve at the origin; $E_{st} =$ stabilized modulus after a number of load cycles; $E_c =$ first-loading secant modulus; here, the modulus is introduced as E_0, which is a function of the temperature).

The damage indexes $D_v{}^T$ (Equation 4) and $D_E{}^T$ (Equation 2) are plotted in Figure 13(a) and (b), while their interdependence stands out in Figure 13(c). For any given damage level, the index $D_E{}^T$ appears to have higher values than $D_v{}^T$ (Figure 13(a) and (b)). For instance, for $f_c^T/f_c^{20} = 0.6$ (Mix M0), the damage

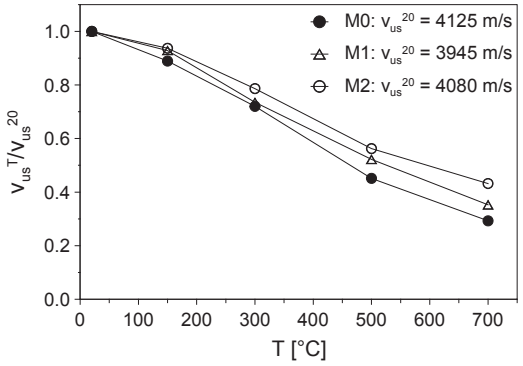

Figure 12. Plots of the normalized velocity of the ultrasonic waves as a function of the temperature. (The velocity was measured along the axes of the concrete cylinders).

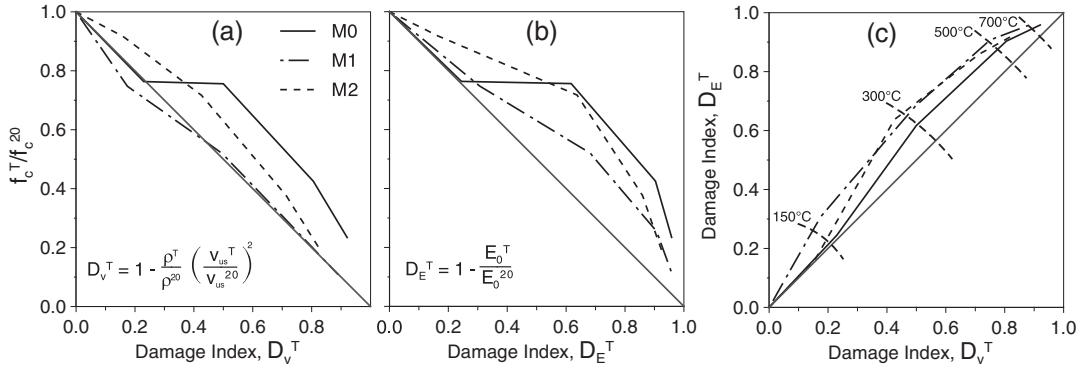

Figure 13. Plots of the damage indexes based on the ultrasonic velocity (a) and on the elastic modulus (b), and correlation between the two indexes (c), for various values of the temperature. E_0 = tangent modulus (=slope of the stress–strain curve at the origin).

index $D_v{}^T$ is close to 0.6, while $D_E{}^T$ is close to 0.8, which means that $D_E{}^T$ is more conservative, as indicated also by the plots of Figure 13(c), where the values of $D_E{}^T$ are always larger than those of $D_v{}^T$.

It is worth noting, however, that (1) the index based on the velocity, $D_v{}^T$, has a better correlation with the heat-affected compressive strength (Figure 13(a)) and (2) the reason why the index based on the modulus is generally larger is that it is measured under load (causing the activation of microdefects and creep), while the index based on the velocity is measured in a no-load situation.

As can be easily understood, *damage indexes* are still a highly debated issue.

9. CONCLUSIONS

The results of this study show that EPS-based concrete is slightly more temperature sensitive than ordinary concrete and weaker in virgin conditions (because of the *empty* volume occupied by EPS particles), but its insulation properties are higher at any temperature up to 500°C, and its mass is significantly smaller.

In particular, the following comments can be made.

Stress–strain curves in compression: both in virgin and residual conditions, at any temperature, the curves exhibit a well-defined linear ascending branch, with the strain at the peak comprised between 1.8–2.5‰ at room temperature and 5.5–8.0‰ at 700°C, as in ordinary concrete, followed by a descending branch that becomes increasingly smoother at high temperature.

Strength and stiffness: the EPS concretes investigated in this study seem to be slightly more temperature sensitive than ordinary concrete in terms of compressive strength and elastic modulus, but the overall behavior is not very different from that predicted by ACI for siliceous and carbonate (calcareous) aggregates, and from the many test results found in the literature for ordinary concrete. As for the tensile strength as a function of the temperature, the normalized curves of EPS concrete and ordinary concrete are very close. In general, increasing the cement content beyond certain limits hardly improves the mechanical performance at any temperature.

Mass loss and thermal diffusivity: adding EPS particles markedly increases the mass dependency on the temperature, as the loss at 700°C is roughly 50% higher in EPS concrete than in ordinary concrete, but does not exceed 10% of the total mass, as confirmed also by EC2; adding EPS particles dramatically reduces concrete thermal diffusivity between 150°C and 500°C, but above 500°C the differences tend to become marginal with respect to ordinary concrete; hence, EPS concrete has very good insulation properties, and its use may increase the fire resistance of any given R/C member or may bring in generalized reductions of the concrete cover for the same fire resistance.

Heat-induced damage: the heat-induced damage—mainly in the form of microcracking and increasing porosity—is effectively described by two *damage indexes* based on the velocity of the ultrasonic waves and on the elastic modulus (at the origin of the stress–strain curve), both quantities being decreasing functions of the temperature. The relationships between the normalized residual strength in compression

and the damage indexes show that the damage index based on the elastic modulus is more conservative than that based on the ultrasonic velocity (at least in a concrete full of voids, like EPS concrete), because for the same temperature (i.e., for the same damage), the values of the former index are always larger. However, the index based on the ultrasonic velocity appears to be more realistic, because of its better correlation with the heat-affected compressive strength in both ordinary and EPS concretes, at any temperature.

Possible effect of aging: although not addressed in this project, aging may or may not affect EPS concrete, with possible consequences on its thermal behavior at high temperature. As a matter of fact, the long-term disappearance of expanded polystyrene inside the concrete is well known; however, contrary to the big polystyrene blocks, whose *sublimation* changes the insulation properties of a concrete member (because convection and cavity radiation replace heat conduction inside the voids), the disappearance of the very small polystyrene beads in EPS concrete cannot—reasonably—change the thermal properties of the material. (This issue still requires a proper investigation).

Last but not least, a few words should be devoted to the fundamental problem of the standing of EPS concrete within the large family of concretes, with specific reference to LWA concrete and ordinary concrete. If strength and stiffness are required, ordinary concrete is the best at any temperature, even in terms of cement demand. If strength and mass reduction are required, with the plus of higher insulation properties, LWA concrete is very appealing. If mass reduction and insulation properties are required, with the plus of using rather inexpensive polymeric beads, EPS concrete is a suitable alternative to LWA concrete at any temperature, with the plus of being *ecological*, because EPS concrete allows the recycling of waste polystyrene. However, for the same strength, EPS concrete requires higher cement contents than both LWA concrete and ordinary concrete, something that balances—or outbalances—the ecological plus of using waste materials. (As a matter of fact, the higher the cement content, the higher the carbon dioxide emissions in the cement-producing plant). Furthermore, material costs and availability are another critical aspect of any comparisons among ordinary, LWA, and EPS concrete: for instance, looking at today's Italian situation and putting cement cost per unit mass equal to one (Portland cement), the costs per unit mass of certified aggregates, structural expanded clay, and EPS beads are close to 1/3, 5, and 30, respectively. Moreover, in the specific case of EPS concrete, the greater content of the additives (like viscosity modifiers) and the need of certain technological expedients (to avoid particles flotation and segregation) increase the total cost per unit volume or mass.

ACKNOWLEDGEMENTS

The authors acknowledge the collaboration of Marco Magnoni, Alessandra Piovan, and Umberto Ruspa, who performed most of the tests in partial fulfillment of the requirements concerning their BS Degree in Civil Engineering. Professor Marisa Pecce of the University of Sannio (Benevento, Italy) is thanked for providing all the specimens and giving suggestions, which were instrumental in securing the success of this project.

REFERENCES

1. ACI 213R-87. Guide for structural lightweight aggregate concrete, ACI Committee 213 (Chairman H.C. Robinson) 2009; 27.
2. Miled K, Sab K, Le Roy R. Particle size effect on EPS lightweight concrete compressive strength: experimental investigation and modelling. *Mechanics of Materials* 2007; **39**:222–240.
3. Perry SH, Bischoff PH, Yamura K. Mix details and material behavior of polystyrene aggregate concrete. *Magazine of Concrete Research* 1991; **43**:71–76.
4. Chen B, Liu L. Properties of lightweight expanded polystyrene concrete reinforced with steel fiber. *Cement and Concrete Research* 2004; **34**:1259–1263.
5. Babu DS, Babu KG, Tion-Huan W. Effect of polystyrene-aggregate size on strength and moisture migration characteristics of light-weight concrete. *Cement and Concrete Composites* 2006; **28**: 520–527.
6. Babu KG, Babu DS. Performance of fly-ash concretes containing lightweight EPS aggregates. *Cement and Concrete Composites* 2004; **26**:605–611.
7. Babu DS, Babu KG, Wee TH. Properties of lightweight expanded polystyrene aggregate concretes containing fly ash. *Cement and Concrete Research* 2005; **35**:1218–1223.

8. Heiser MJ, Hosny A, Rizkalla SH, Zia P. Bond and shear behavior of concrete beams containing lightweight synthetic particles. *ACI Structural Journal* 2011; **108**(6):698–705.
9. Babu KG, Babu DS. Behaviour of lightweight expanded polystyrene concrete containing silica fume. *Cement and Concrete Research* 2003; **33**:755–762.
10. Trussoni M, Hays CD, Zollo RF. Comparing lightweight polystyrene concrete using engineered or waste materials. *ACI Materials Journal* 2012; **109**(1):101–107.
11. Blanco F, García P, Mateos P, Ayala J. Characteristics and properties of lightweight concrete manufactured with cenospheres. *Cement and Concrete Research* 2000; **30**:1715–1722.
12. Bouvard D, Chaix JM, Dendievel R, Fazekas A, Letang JM, Peix G, Quenard D. Characterization and simulation of microstructure and properties of EPS lightweight concrete. *Cement and Concrete Research* 2007; **37**:1666–1673.
13. Le Roy R, Parant E, Boulay C. Taking into account the Inclusions' size in lightweight concrete compressive strength prediction. *Cement and Concrete Research* 2005; **35**:770–775.
14. Miled K, Le Roy R, Sab K, Boulay C. Compressive behavior of an idealized EPS light-weight concrete: size effects and failure mode. *Mechanics of Materials* 2004; **36**:1031–1046.
15. Pecce M, Ceroni F, Bibbò F, Acierno S. Bond behaviour of zinc-coated steel bars embedded in concrete elements with EPS. *Proceedings of the 4th International Conference "Bond in Concrete"* 2012, (ed. by Cairns JW, Metelli G and Plizzari GA), Brescia (Italy), June 17-20; **2**: 861–868.
16. Bamonte P, Lo Monte F, Gambarova PG, Pecce M. High-temperature behavior of reduced-mass concrete containing expanded-polystyrene syntherized particles. *Proceedings 2013 fib Symposium on "Engineering a Concrete Future: Technology, Modeling and Construction"* 2013, Tel Aviv (Israel), April 22-24: 61–64.
17. Fares H, Noumowé A, Remond S. Self-consolidating concrete subjected to high temperature: mechanical and physico-chemical properties. *Cement and Concrete Research* 2009; **39** : 1230–1238.
18. Felicetti R, Gambarova PG, Bamonte P. Thermal and mechanical properties of light-weight concrete exposed to high temperature. *Fire and Materials* 2012; **37**(3):200–216.
19. EN 1992-1-2. 2004. Eurocode 2 - design of concrete structures - part 1-2: general rules - structural fire design. *European Committee for Standardization (CEN)* 2004, Brussels (Belgium).
20. ISO 5017. 1998. Dense shaped refractory products - determination of bulk density, apparent porosity and true porosity. *International Organization for Standardization (ISO)* 1998, Genève (Switzerland).
21. Gallé C. Effect of drying on cement-based materials pore structure as identified by mercury intrusion porosimetry: a comparative study between oven-, vacuum-, and freeze-drying. *Cement and Concrete Research* 2001; **31**:1467–1477.
22. Felicetti R. Assessment of the equivalent thermal diffusivity for fire analysis of concrete structures. *Proceedings Fib Task Group 4.3 Workshop Fire Design of Concrete Structures* 2008 (ed. by Rodriguez JP, Khoury GA, Hoj NP) Coimbra (Portugal), November 8-9, 2007: 149–158.
23. ACI 216-1.07. Code requirements for determining fire resistance of concrete and masonry construction assemblies. *Report by Joint ACI/TMS Committee 216* 2007, 32.
24. Phan LT, Carino NJ. Review of mechanical properties of HSC at elevated temperature. *ASCE - Journal of Materials in Civil Engineering* 1998; **10**(1):58–64.
25. Lemaître J. A Course on Damage Mechanics. Springer Verlag, 1992.
26. Di Prisco M, Felicetti R, Gambarova PG. On the evaluation of the characteristic length in high-strength concrete. *Proceedings of the International Conference on High-Strength Concrete – ASCE* 1997 (ed. by Azizinamini A, Darwin, French C) Kona, Hawaii (USA): 377–390.
27. Bamonte P, Felicetti R. High-temperature behaviour of concrete in tension. *Structural Engineering International Association for Bridge and Structural Engineering – IABSE* 2012; **22**(4): 493–499.